Electronic Supplementary Material (ESI) for Physical Chemistry Chemical Physics.
This journal is © the Owner Societies 2018

Supporting Information For

Determination of Accurate Backbone Chemical Shift Tensors in Microcrystalline Proteins by Integrating MAS NMR and QM/MM

Matthew Fritz[1,2], Caitlin M.Quinn[1,2], Mingzhang Wang[1,2], Guangjin Hou[1], Xingyu Lu[1,2], Leonardus M. I. Koharudin[2,3], Jochem Struppe[4], David A. Case[5], Tatyana Polenova[1,2*], and Angela M. Gronenborn[2,3*]

[1]Department of Chemistry and Biochemistry, University of Delaware, Newark, DE 19716, United States; [2]Pittsburgh Center for HIV Protein Interactions, University of Pittsburgh School of Medicine, 1051 Biomedical Science Tower 3, 3501 Fifth Ave., Pittsburgh, PA 15261, United States; [3]Department of Structural Biology, University of Pittsburgh School of Medicine, 3501 Fifth Ave., Pittsburgh, PA 15261, United States; [4]Bruker Biospin Corporation, 15 Fortune Drive, Billerica, MA, United States; [5]Department of Chemistry and Chemical Biology, Rutgers University, 174 Frelinghuysen Road, Piscataway, NJ 08854-8087, United States

***Corresponding authors:** Angela M. Gronenborn, Department of Structural Biology, University of Pittsburgh School of Medicine, 3501 Fifth Ave., Pittsburgh, PA 15260, USA, Tel.: (412) 648-9959; Email: amg100@pitt.edu; Tatyana Polenova, Department of Chemistry and Biochemistry, University of Delaware, Newark, DE, USA, Tel.: (302) 831-1968; Email: tpolenov@udel.edu

Table S1. Experimental and calculated principal components of the CSA tensor for $^{15}N^{H}$ atoms for microcrystalline OAA

	Experimental			OLYP/TZVP		
Residue	δ_{11}	δ_{22}	δ_{33}	δ_{11}	δ_{22}	δ_{33}
L3	214.26	89.93	68.27	224.69	112.59	47.25
V6	219.99	94.63	71.39	226.43	101.35	56.89
A15	225.34	85.96	68.50	222.83	91.28	62.68
P16	222.47	135.02	47.57	232.94	138.24	46.67
E24	212.59	92.03	69.75	217.63	95.85	56.03
I25	207.55	97.07	69.57	213.40	102.61	55.22
V33	214.78	89.34	64.25	225.07	104.15	51.57
V34	208.42	76.03	52.09	219.43	78.17	55.83
I36	205.06	85.00	65.94	215.01	95.16	48.89
N37	223.69	88.88	64.74	225.95	93.57	52.12
T50	222.52	75.62	65.49	222.74	79.63	59.34
M51	211.22	80.52	56.11	205.70	81.54	45.88
T52	204.55	81.36	56.21	204.95	84.68	40.67
Y53	222.81	96.20	69.75	228.80	117.71	49.59
P58	217.90	132.31	46.72	233.75	125.62	42.42
I59	217.65	84.42	53.95	210.41	83.17	44.88
F61	217.91	88.09	66.95	239.95	91.14	78.93
A63	215.00	92.82	62.83	214.61	91.71	53.24
T64	211.63	81.25	56.62	222.23	100.40	47.61
L66	224.55	93.56	70.24	222.88	100.24	51.66
D80	197.53	88.45	65.80	218.20	96.88	46.02
A82	225.34	85.96	68.50	218.73	90.90	61.85
P83	222.47	135.02	47.57	235.11	134.36	48.51
H85	206.19	86.93	61.21	210.70	92.67	49.67
I91	209.22	92.67	69.66	213.13	89.95	57.83
L92	210.86	91.10	68.45	207.57	101.33	54.89
S94	200.22	77.27	56.63	224.58	101.41	49.65
V100	214.78	89.34	64.25	218.42	77.84	41.20
V101	208.42	76.03	52.09	218.42	77.84	54.49
I103	205.06	85.00	65.94	214.83	94.94	48.48
N104	223.69	88.88	64.74	224.47	93.40	51.55
T117	222.52	75.62	65.49	226.65	78.94	61.83
M118	211.22	80.52	56.11	211.46	80.94	43.66
T119	204.55	81.36	56.21	209.72	84.29	42.23
Y120	222.81	96.20	69.75	230.82	118.16	51.88
P125	217.90	132.31	46.72	233.37	125.88	42.56

I126	217.65	84.42	53.95	208.88	82.28	44.89
F128	217.91	88.09	66.95	237.39	90.28	66.65
K129	227.05	94.50	71.85	228.90	90.85	58.59
T133	217.92	91.17	65.52	206.24	78.71	30.85

Table S2. Experimental and calculated principal components of the CSA tensors for $^{13}C^{\alpha}$ atoms for microcrystalline OAA

	Experimental			OLYP/TZVP		
Residue	δ_{11}	δ_{22}	δ_{33}	δ_{11}	δ_{22}	δ_{33}
V6	82.85	61.93	41.07	81.35	56.20	43.29
E7	77.17	54.57	32.09	77.30	49.80	35.71
A15	72.01	50.94	30.02	76.34	51.60	28.13
P16	85.63	62.78	40.35	93.80	61.18	38.05
G20	61.87	43.67	28.05	74.14	42.58	18.84
E24	77.13	55.84	35.34	78.72	49.70	37.28
I25	81.21	60.20	39.43	79.56	45.05	44.42
V33	82.97	64.21	46.17	74.63	61.20	48.85
V34	85.67	59.68	34.29	84.87	62.15	34.29
I36	83.64	62.66	41.71	81.31	53.17	48.01
V38	82.33	58.37	34.44	81.18	50.77	38.07
T50	84.89	56.88	37.75	82.71	50.91	41.29
M51	77.15	55.30	33.68	76.70	51.13	37.09
T52	78.72	61.71	44.70	79.51	53.76	47.83
Y53	80.71	58.98	38.84	77.57	56.13	42.39
P58	85.35	63.38	41.92	85.23	70.28	35.04
I59	85.35	59.45	35.08	84.51	52.39	39.16
F61	78.32	56.70	36.67	71.07	56.48	37.45
A63	74.03	50.60	27.26	72.13	50.82	31.86
T64	84.84	60.47	37.88	77.81	53.73	45.70
L66	79.56	55.14	31.80	81.37	51.78	35.15
E72	80.09	58.36	36.64	73.03	51.44	37.71
E74	77.17	54.57	32.09	76.37	50.48	34.69
G78	71.09	45.60	20.39	74.40	46.83	16.11
D80	76.51	47.20	47.20	72.01	61.00	37.26
A82	72.01	50.94	30.02	77.42	50.55	28.29
P83	85.63	62.78	40.35	92.00	61.82	35.67
W84	80.57	57.00	35.53	79.87	53.94	32.59
H85	76.91	52.59	32.08	78.49	52.50	35.84
I91	84.20	60.56	38.87	81.75	53.00	42.80
L92	75.53	54.73	34.43	72.67	46.94	36.84
V100	82.97	64.21	46.17	74.19	59.51	49.51
V101	85.67	59.68	34.29	84.40	62.59	34.03
I103	83.64	62.66	41.71	81.18	53.15	48.21
V105	82.33	58.37	34.44	80.81	50.81	38.35

T117	84.89	56.88	37.75	83.52	50.92	41.18
M118	77.15	55.30	33.68	73.55	52.15	32.61
T119	78.72	61.71	44.70	80.07	54.20	47.89
Y120	80.71	58.98	38.84	77.78	56.73	42.26
G124	75.09	43.44	29.40	76.65	44.69	16.06
P125	85.35	63.38	41.92	84.48	70.04	35.02
I126	85.35	59.45	35.08	84.98	52.27	38.90
F128	78.32	56.70	36.67	75.48	52.64	41.83
K129	84.60	54.92	46.99	74.62	52.84	39.18
T133	80.13	54.99	54.93	80.32	63.22	41.76

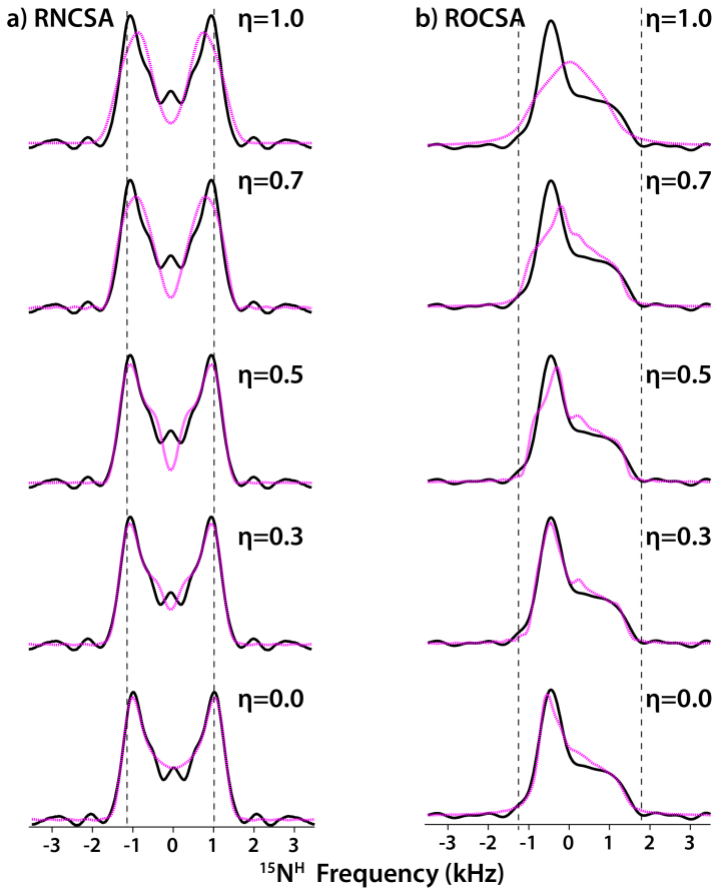

Figure S1. $^{15}N^{H}$ $R14_2^5$-RNCSA (left) and ROCSA (right) lineshapes for I36. Experimental data are shown as solid black lines, best-fit lineshapes using different asymmetry parameters, η_σ – as dashed magenta. Note that η_σ are reliably determined from the ROCSA lineshapes, while the $R14_2^5$-RNCSA lineshapes are not sensitive to changes below an asymmetry parameter of 0.5.

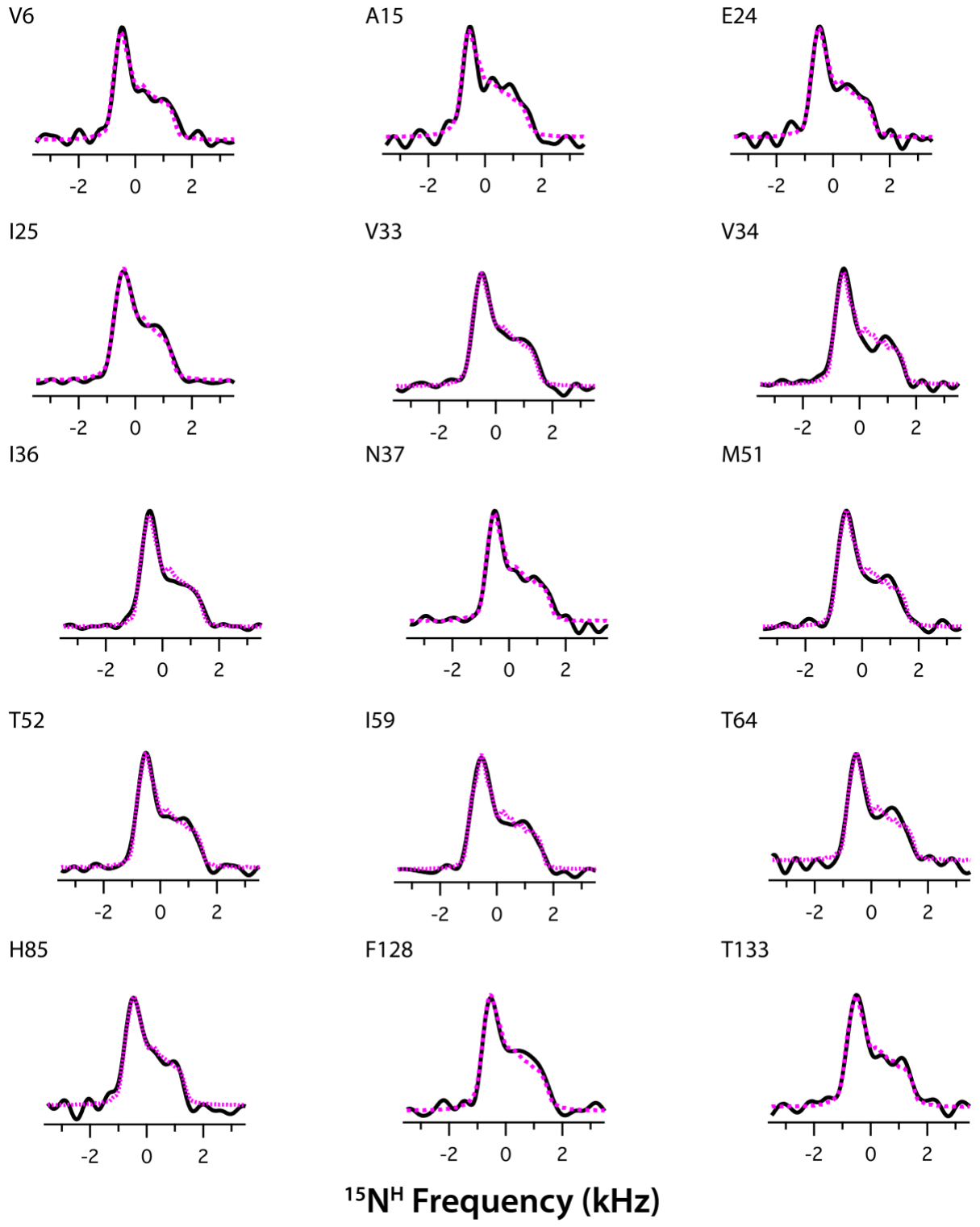

Figure S2. $^{15}N^{H}$ ROCSA lineshapes for representative residues of OAA. Experimental data are shown as solid black lines, best-fit lineshapes are shown in dashed magenta lines.

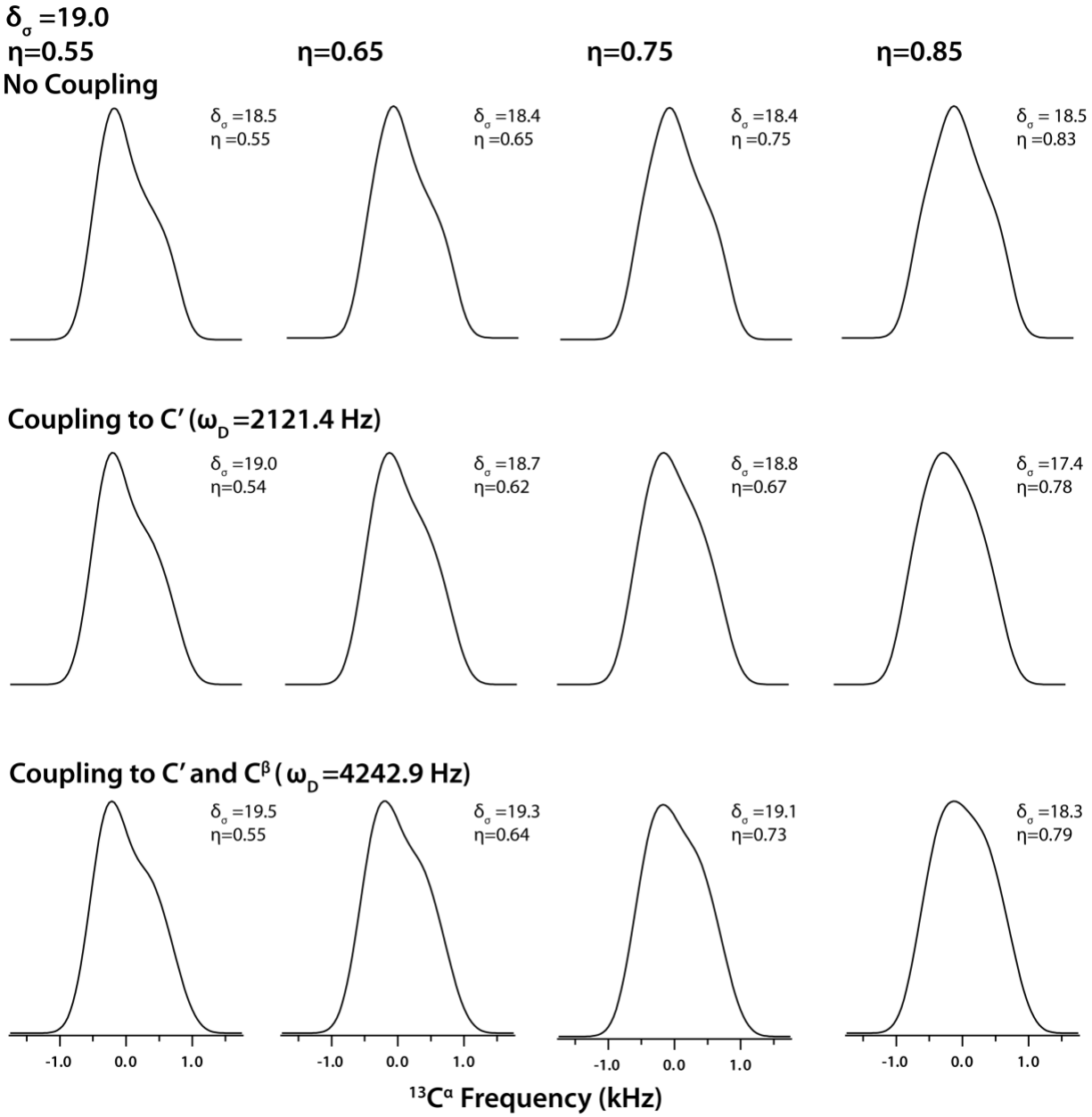

Figure S3. Effects of ^{13}C-^{13}C homonuclear dipolar interactions on the simulated $^{13}C^{\alpha}$ ROCSA lineshapes. Theoretical lineshapes were generated in SIMPSON using a reduced anisotropy of 19.0 and asymmetry parameters of 0.55, 0.65, 0.75, and 0.85. At high values of the asymmetry parameter, broadening caused by homonuclear dipolar interactions can potentially interfere with assigning a sign to the reduced anisotropy. It should be noted that the magnitude of the reduced anisotropy is underestimated when fitting experimental ROCSA lineshapes in the absence of the dipolar coupling.

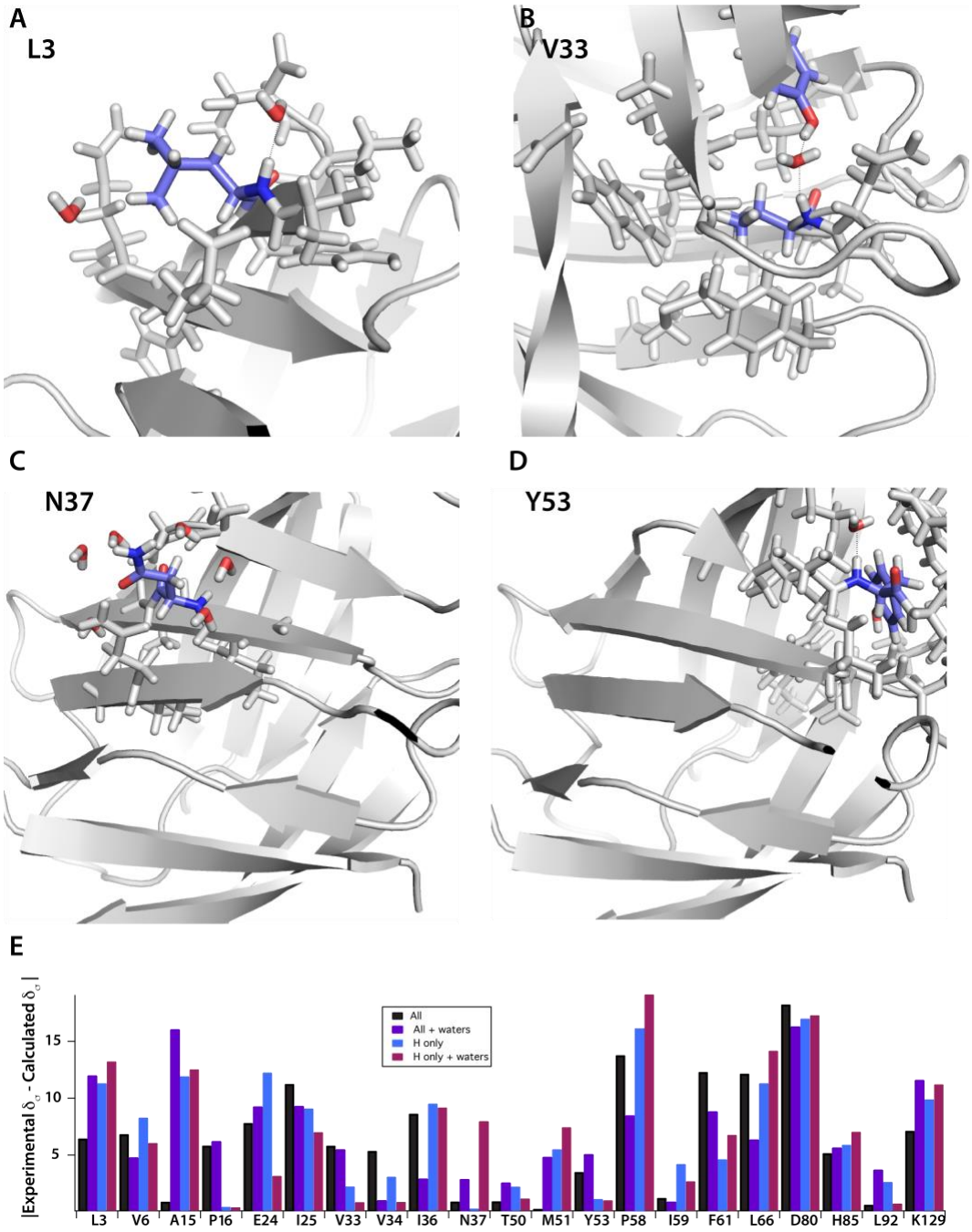

Figure S4. Structural details of selected regions in OAA. Relevant residues and waters are shown in color and hydrogen bonds are indicated. A) L3, surrounding residues and crystallographic water; note the hydrogen bond between the backbone amide of L3 and a bulk water. B) The hydrogen bond bridge formed between V33 amide, a crystallographic water, and the side chain of Y4. C) N37 side chain surrounded by bulk water. D) The hydrogen bond between Y53 amide and water. E) Analysis of the differences in experimental versus calculated reduced anisotropy parameters for selected residues. All atoms (black), all atoms plus water molecules (purple), H atoms only (blue) and H-atoms plus waters (magenta) were included in the minimization.

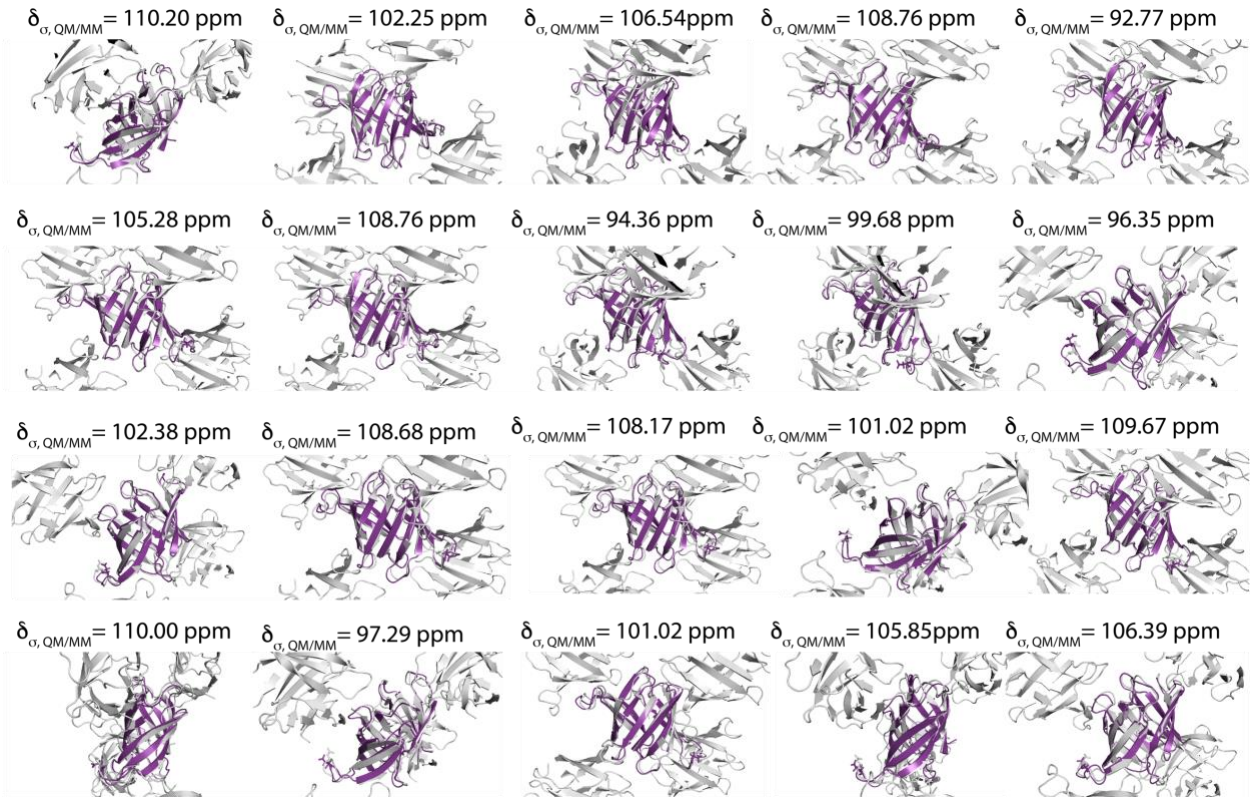

Figure S5. $^{15}N^{H}$ reduced anisotropy of D80 as a function of conformation. The twenty lowest energy solution NMR conformations (PDB ID:2MWH) are shown in purple superimposed onto the crystallographic structure highlighting the quaternary contacts. At the top left is conformation 1 and the conformations are ordered by increasing energy from left to right and top to bottom. Despite the averaging over the ensemble, the motional attenuation of the $^{15}N^{H}$ reduced anisotropy of D80 is not captured. Thus, longer MD trajectories may be necessary.

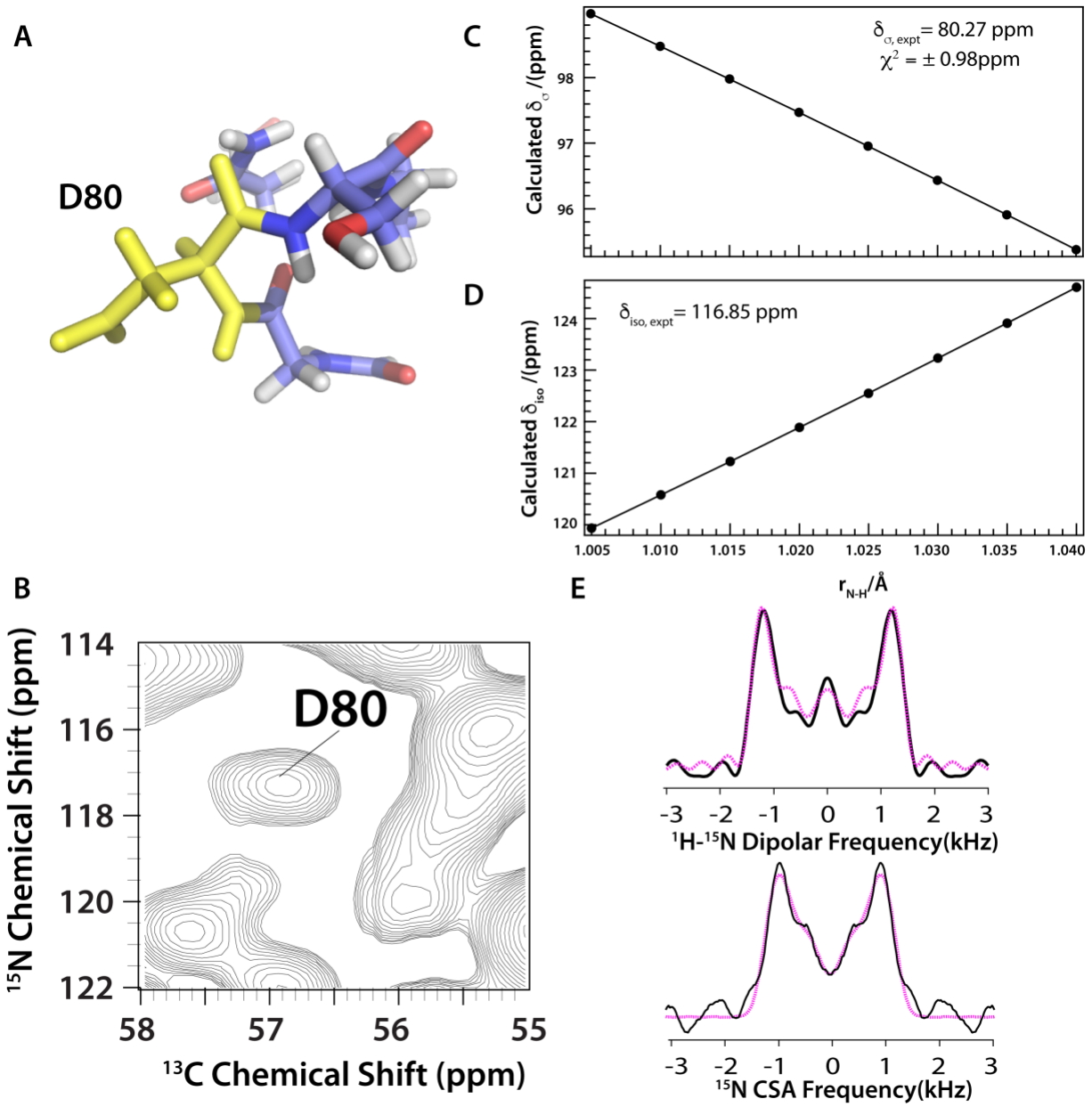

Figure S6. Influence of the N-H bond length on the QM(DFT)/MM calculated $^{15}N^{H}$ CSA parameters in residue D80. **A:** Geometry-optimized QM region around D80. **B:** Expansion around the D80 resonance in the 2D NCA spectrum, illustrating that no overlap with other resonances exists. **C, D:** The QM(DFT)/MM calculated $^{15}N^{H}$ CSA parameters δ_σ and δ_{iso}, plotted vs. the N-H bond length. **E:** PARS ^{1}H-^{15}N dipolar (top) and ^{15}N RNCSA (bottom) lineshapes for D80. The experimental lineshapes are shown in black, simulated in magenta.